Numerical model for estimating RF-induced heating on a pacemaker implant during MRI. Experimental validation.

Eugenio Mattei, Giovanni Calcagnini, Federica Censi, Michele Triventi, and Pietro Bartolini

***Abstract*— Magnetic resonance imaging (MRI) may cause tissue heating in patients implanted with pacemakers or cardioverters/defibrillators. As a consequence, these patients are often preventatively excluded from MRI investigations. The issue has been studied for several years now, in order to identify the mechanisms involved in heat generation, and define safety conditions by which MRI may be extended to patients with active implants. In this sense, numerical studies not only widen the range of experimental measurements, but model a realistic patient's anatomy on which it is possible to study individually the impact of the many parameters involved. In order to obtain reliable results, however, each and every numerical analysis needs to be validated by experimental evidence. Aim of this paper was to design and validate through experimental measurements an accurate numerical model able to reproduce the thermal effects induced by a birdcage coil on human tissues containing a metal implant, specifically a pacemaker. The model was then used to compare the right-versus-left pectoral implantation of a pacemaker, in terms of power deposited at the lead tip. This numerical model may also be used as reference for validating simpler models in terms of computational effort.**

***Index Terms*—Magnetic Resonance Imaging, RF fields, Pacemaker, Specific Absorption Rate,**

I. Introduction

Magnetic resonance imaging (MRI) uses non ionizing radiation, and is daily applied in clinical and interventional diagnosis. During MRI of patients implanted with metal devices, e.g., pacemakers (PMs), brain stimulators, cochlear implants, there is the risk of radiofrequency (RF) heating. The RF field generated during the MRI procedure may induce electrical currents from the implant towards biological tissue, which may cause a local increase in the specific absorption rate (SAR), tissue heating and damage. In-vivo and in-vitro experimental studies have shown the complexity of the electromagnetic fields induced within MRI RF coils, and described many aspects that influence temperature increase around the implant [1-6]. In particular, implant configuration -which in the clinical practice may significantly vary from patient to patient- seems to play a major role in MRI-induced heating.

All this, together with the growing recognition of the role played by tissue-coil interactions, have rendered it clear that numerical techniques based on full-wave methods can provide essential information for understanding the behavior of RF coils when they are loaded with biological structures [7].

Computational tools based on full-wave methods are successfully used in RF coil feasibility studies, which are extremely difficult to carry out in experimental settings. As such, for whole-body human applications, computational electromagnetics can be effectively used to design and evaluate RF coils before they are constructed and experimentally tested. Below 1.5 Tesla, the traditional design of RF head coils for MRI systems has been based on lumped elements circuit concepts. As B_0 fields increase, however, this approach becomes inadequate since coil dimensions are a significant fraction of the operational wavelength. Under these conditions, the currents in the coil do not behave in a manner in which circuit analysis can predict [8]. Consequently, the use of computational electromagnetic techniques, such as the finite difference time domain (FDTD) method [9], has recently flourished for modeling RF coils [8-11], including birdcage [12] and transverse electromagnetic (TEM) [13] resonators. It has already been shown that the optimization of today's high-field RF coils, or the design of new coils, will heavily rely upon numerical modeling [14,15]. In any case, numerical analyses need to be validated by experimental evidence: for this reason, if one wants to use a computational tool to study the interaction between an electromagnetic field and a metallic structure implanted in biological tissues, experimental measurements have to be done to ensure the validity of the model.

Aim of this paper was to design and validate through experimental measurements a numerical model able to reproduce the thermal effects induced by a MRI RF coil on human tissues containing a metal implant, specifically a PM. We chose to validate the model of a 16-leg, low-pass, birdcage coil, since birdcage coils are currently the most used in 1.5T MRI scanners. The model was then used to compare the right-versus-left pectoral implantation of a PM in terms of power deposited at the lead tip, and identify worst-case conditions.

Manuscript submitted December 22, 2009.) This study was partially funded by the 2007 Italian Ministry of Health grant.

E. Mattei, G. Calcagnini, F. Censi, M. Triventi, and P. Bartolini are with the Department of Technology and Health, Italian National Institute of Health, Rome, Italy (e-mail: eugenio.mattei@iss.it; giovanni.calcagnini@iss.it; federica.censi@iss.it; michele.triventi@iss.it; pietro.bartolini@iss.it).

II. Materials and Methods

The structure chosen for the RF coil was a 16-leg, low-pass, birdcage coil tuned at 64 MHz, with a quadrature sinusoidal excitation (two signals 90°-shifted in both space and time).
The same structure implemented as both numerical model and physical prototype provided us with a direct mean for validating the results of the numerical analysis, thus reducing the number of variables typically involved in other validation procedures. The numerical model was validated versus two physical coils: a head-sized coil and a whole-body coil. The former provides validation in terms of electrical parameters (return loss, RL, and currents along the legs), the latter, in terms of induced SAR on metal implants (figure 1).

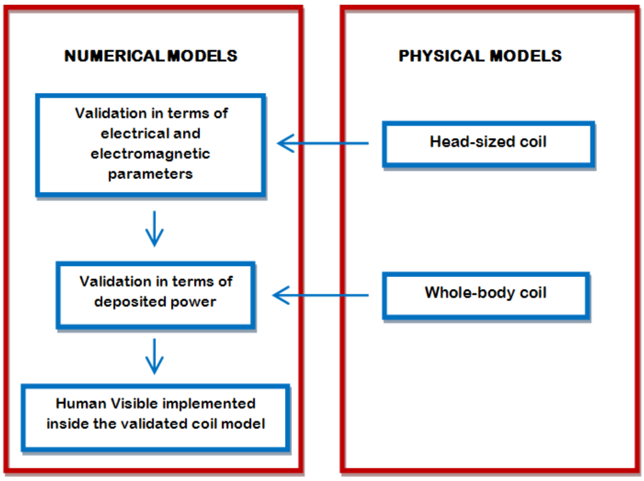

Fig. 1. Main steps in the design and validation of the numerical model.

A. *Head-sized coil*

A commercial 3D-CAD software (SolidWorks, SolidWorks Corporation, USA) was used to design the scheme common to both the numerical model and the prototype of the head-sized birdcage. The components of the coil are big enough to be easily implemented in the FDTD environment, but also suitable to be handled in an ordinary mechanical workshop. In particular, the coil is made up of 16 cylindrical copper legs (diameter = 6 mm, height = 30 cm) and two external aluminum rings (12 mm x 8 mm rectangular section) of 30 cm internal diameter. In each leg, three 1 mm gaps -in the middle and just before the connection with the two rings- host the tuning capacitors. Another three PVC rings supply the structure with more stability at the points where the capacitors are to be placed (figure 2). The coil is excited through two RF ports placed 90° apart on one of the two aluminum rings, between the ring and one of the legs.

The 16-leg structure with three capacitors per leg was derived from the usual scheme adopted by birdcage coil manufacturers; if compared with the standard birdcage model, with a single capacitor per leg, our solution better reproduces the actual behavior of an experimental birdcage coil and the distributed capacitance that is obtained along the coil legs (typically made up of metal plates separated by dielectric material). In addition, this structure is the same as the whole-body coil that was used in the experimental validation of the model in terms of induced SAR (see paragraph 2.2).

A.1 Numerical Model

We imported the CAD file with the geometry (Figure 2 a) of the coil into an FDTD environment, using a commercial FDTD software (SEMCAD X, version 14.0, SPEAG, Zurich) which has a variable grid (graded-mesh) generator. The simulations were run on a personal computer with a 2.4 GHz, 64-bit processor, 3 GB RAM, and Windows XP operating system. An accelerator card (aXware Card V1.5) was used to speed up the performance of the numerical solver. We conducted a preliminary broadband analysis to find the value of the tuning capacitors that renders the coil resonant at 64 MHz (the RF used in the 1.5 T clinical scanner). The coil was excited by an impulse signal with frequency content in the band 40-80 MHz applied to one of the RF ports. The other port was terminated into a 50 Ohms load. We found that a capacitance of 17.2 pF rendered the coil resonant at 64MHz.

To obtain a circular polarized magnetic field on the transversal plane of the coil, i.e., the typical field distribution inside MRI RF coils, two quadrature signals (90° phase shifted) were applied to the RF ports.

The amplitude of the quadrature signals was adjusted to have a total forward power of 470 mW.

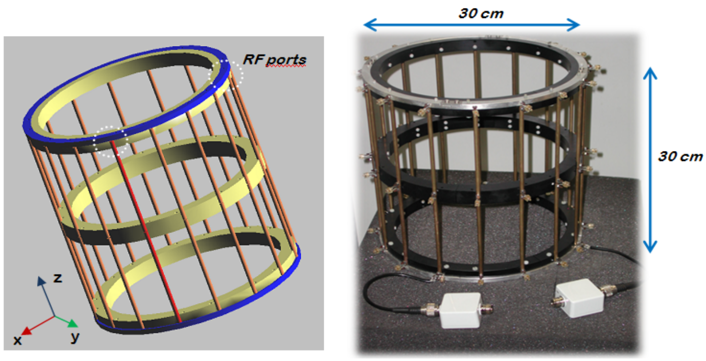

Fig. 2. a) Design of the a 16-leg, low-pass head-sized birdcage coil in a 3D CAD environment. b) Physical model of the 16-leg, low-pass birdcage coil.

A.2 Physical Model

Figure 2 b), is a picture of the head-sized coil. The tuning capacitors (high-Q Teflon, *ARCO-TRM* 461) were tuned with an LRC meter (4263B, *Hewlett-Packard*, USA) to the same value resulting from the broadband simulation.

The two RF ports were excited by quadrature signals from a signal generator (SMT 06, *Rhode & Schwartz*, Germany) connected to an RF amplifier (RF 06100-6, *RFPA*, France). The 90° shift between the two signals feeding the coil was obtained by a 90° phase splitter (SMY-64-90, *SAMA* S.r.l., Rome, Italy), whose outputs were balanced to ground by a pair of single-frequency baluns (SMZ-64-5070, *SAMA* S.r.l., Rome, Italy). The output power towards the coil was monitored in real time with an RF power meter (NRT, Z14, *Rhode & Schwartz*, Germany). The amplitude of the input signals was set to have a total forward power of 470 mW.

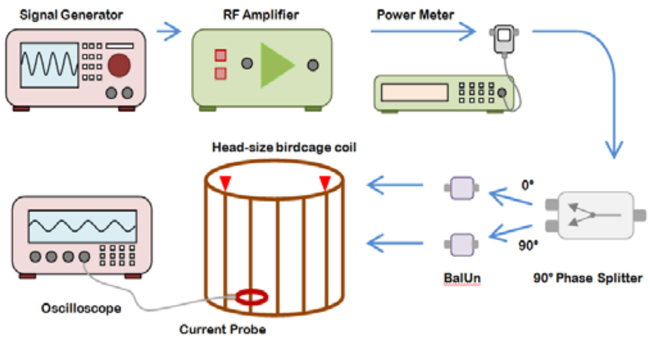

Fig. 3. Sketch of the experimental set-up for current amplitude and phase measurements on the head-sized birdcage coil.

A.3 Validation of the Numerical Model

The head-sized birdcage coil numerical model was validated in terms of RL and currents along the legs.

We compared the measured vs. computed RL as a function of frequency. In the coil prototype, the RL was measured by a handheld vector network analyzer (Bravo MRI II, *AEA Technology* Inc, USA).

Current amplitude and phase at each leg were measured with a clamp-on broadband current probe (BCP-512, *A.H. System,* USA) connected to a high-frequency oscilloscope (WavePro 7300A, *LeCroy*, USA). Figure 3 illustrates the experimental set-up. Results have been reported as mean value and standard deviation of 10 repeated measurements.

B. Whole-body coil

Once the head-sized coil numerical model was experimentally validated, it was scaled to match the dimensions of a whole-body birdcage coil (length = 62 cm; diameter = 62 cm), with the same overall structure as for the head-sized one. The whole-body coil can be loaded with a human trunk phantom and used to study the RF-induced heating on metal implants in realistic configurations.

B.1 Numerical Model

The numerical model of the whole-body coil was the same as the one described for the head-sized coil, but for dimensions and value of the tuning capacitors. The broadband simulation led to set the capacitors at 70 pF to render the coil resonant at 64MHz. A rectangular box (35x61x11.5 cm) was placed inside the coil, simulating the standard gel saline phantom used in MRI implants heating tests [16]. The dielectric properties of the rectangular box were chosen according to the ASTM standard (conductivity=0.69 Sm^{-1}; permittivity=79). The coil was excited by quadrature signals, whose level was adjusted to produce an average SAR of 1 WKg^{-1} inside the rectangular box.

Implants inside the rectangular box were modeled with insulated metal wires of different path and length. The wires had a radius of 0.5 mm with an insulated sheath of 0.5 mm and a bear tip of 1mm.

B.2 Physical Model

The RF coil had the same dimensions as its numerical counterpart. Two tuning capacitors were placed on each leg, between the leg and the rings. Each leg was made of two parallel copper plates, divided by a thin layer of dielectric material, resulting in a distributed capacitance. This coil structure is commonly used in 1.5 T clinical MRI. The coil was fed by a quadrature power splitter so as to produce a circularly polarized B1 field. The birdcage coil was housed in an anechoic chamber and fed by a RF amplifier that delivers over 130 Watts at 64 MHz. A rectangular box phantom (35x61x19 cm) was filled with a gel saline solution (2% by weight Hydroxyethylcellulose, HEC, 0.4% NaCl) for a total volume of 24.6 l (24.7 kg). Solution conductivity was about 0.7 Sm-1 at 64 MHz, and 79 permittivity. The chosen amount of HEC allowed implants to be placed in the gel, moved and replaced, but also provided a barrier to rapid thermal convection. A 26×18 cm grid was submerged in the gel to support the implants and maintain a consistent separation distance between the metallic structures, the phantom gel surface and the temperature probes. The grid was adjusted so that the top of the implant was positioned 2 cm below the phantom surface.

The box was thermally sealed with 2.6 cm of rigid foam and placed on a wooded board at about 10 cm from the bottom of the RF coil. The foam allowed us to perform calorimetry studies to set the amplitude of the quadrature signals to have an averaged whole body SAR of 1Wkg^{-1} .

B.3 Validation of the Numerical Model

The whole-body coil model was validated in terms of local SAR deposition at the tip of metal implants.

Local SAR deposition was calculated from the E-field estimated by the model. SAR was calculated as described in [16], over a 1mg mass. A 1 mg mass was chosen as a trade-off between a volume small enough to significantly account for local SAR value, but big enough to prevent misleading results due to computational errors [17].

In the physical model, SAR was estimated from the rate of temperature rise recorded at the implant tip, according to [18]. Fluoroptic probes (SMM probes, *Luxtron,* Model 3100, California, USA) were used to measure the temperature.

Local SAR was numerically computed and experimentally measured for the following implant configurations:

1) Two 62-cm long metal wires shaped to simulate the two typical implants paths for a PM lead, corresponding to a left and right pectoral implant position;

2) The same 62-cm long metal wires used to simulate the left and right pectoral implants, but reversed in a symmetric configuration with respect to the main axes of the phantom;

3) Three wires of different lengths (15cm, 20 cm, 49 cm), close to the phantom's edge;

4) Three 25-cm long wires placed in the middle, half-way and close to the phantom's edge.

Experimental measurements were performed at the CDRH of the FDA; further details can be found in [6].

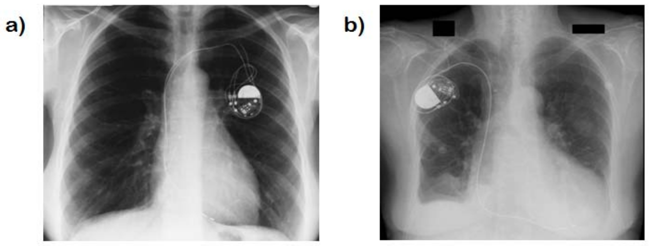

Fig. 4. RX images of PM-implanted patients: a) left pectoral implant; b) right pectoral implant.

C. Human Visible dataset

We integrated the whole-body coil model with a “Human Visible dataset” (HVD), which can reproduce 34 different human tissues with a spatial resolution of 2 mm.

We reproduced two typical PM implants inside the human trunk model: in one, the PM chassis was located in the left pectoral region, immediately under the skin, the lead inserted into the left subclavian vein, left brachoencefalic vein, superior cava, right atrium, down to the right ventricle, where the tip leaned against the heart wall. The other was a right-pectoral PM implant where the lead reached the right atrium through the right subclavian vein, right brachoencefalic vein, and superior cava. The path from the right atrium to the right ventricle was the same for both configurations. Implant geometries and positioning were derived from RX images of implanted patients (figure 4). The FDTD model of the birdcage coil and the HVD with the PM implant required a very high spatial resolution: in particular, the graded mesh had to be very fine (min. step=0.4 mm) all over the area covered by the implant, in order to simulate the insulated sheath all along the lead path. Figure 5 shows the final FDTD model.

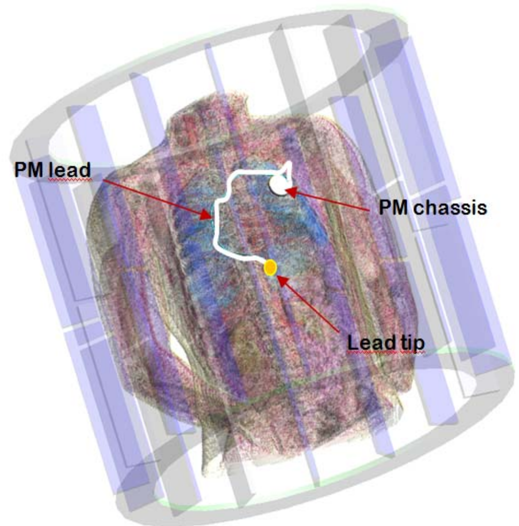

Fig. 5. FDTD model of the whole-body birdcage coil and of the Visible Human dataset implanted with a PM.

III. Results

A. Validation of the head-sized model. RL coefficient and current measurements

The physical head-sized birdcage coil was compared to its equivalent numerical implementation in terms of RL coefficient, and current amplitude and phase along the legs. Figure 6 reports RL vs. frequency computed for the numerical and physical models. By setting all the tuning capacitors at the same value (17.2 pF) in both models, it was possible to match the resonance at the radiofrequency typically used in 1.5T MRI scanners (i.e. 64 MHz). For the broadband characterization of the coil, single-source excitation was applied to one of the RF ports, the other terminated into a 50 Ohms load.

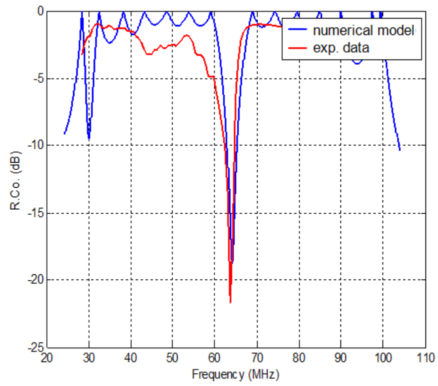

Fig. 6. Reflection coefficient computed in the numerical model and by experimental measurements on the head-sized birdcage coil. The resonance at 64 MHz is obtained by tuning the capacitors to 17.2 pF.

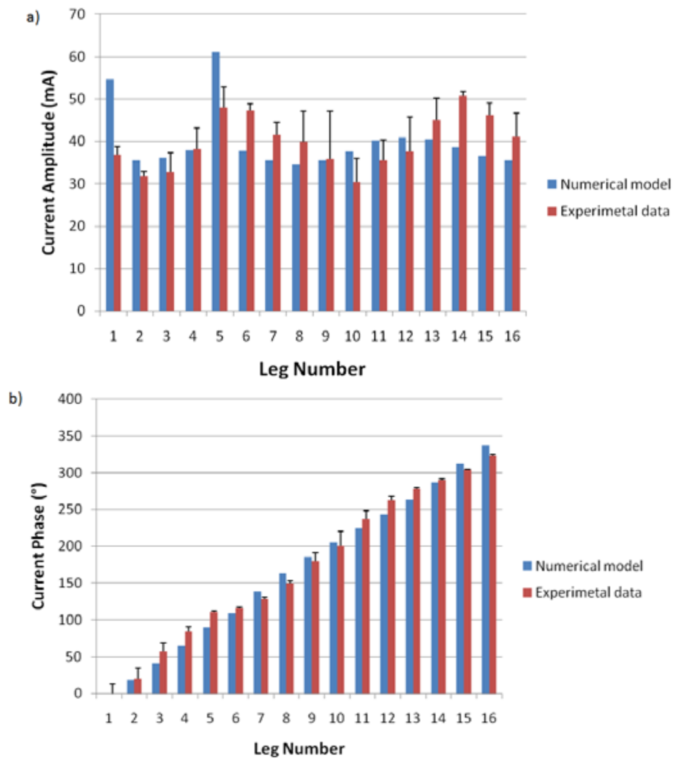

Fig. 7. Current amplitude (a) and phase (b) at the legs of the birdcage coil: comparison between the numerical and physical models of the head-sized coil. The two 90°-shifted RF signals were applied at legs 1 and 5. Phase distribution was normalized assuming that phase was 0° for the current in leg 1. Experimental data are reported as mean value and standard deviation of 10 repeated measurements.

In a second set of measurements, we compared current amplitude and phase at each of the 16 legs of the coil. The 90° phase splitter was used to generate a quadrature excitation signal and a circular-polarized magnetic field inside the coil. Figure 7 summarizes the results.

B. *Validation of the whole-body model. SAR measurements*

Besides RF measurements, we also validated the FDTD model of the birdcage coil in terms of deposited power in a dielectric domain with thin metal wires inside. We used the same experimental dataset as above [6].

In particular, we modeled a rectangular box (with dimensions and physical properties equal to the rectangular-shaped phantom used for the experimental measurements) implanted with thin metallic wires that differed in shape, length and location (figure 8).

Experimental and computed data were consistent: wires with the same shape and length but differently oriented induced different heating behaviour (figure 8, a and b). The highest temperature increase was obtained when wire length was close to the theoretical resonance value at 64 MHz (≈ 26 cm, figure 8, c). The closer the wire to the edge of the phantom, the higher the heating induced at the tip (figure 8, d).

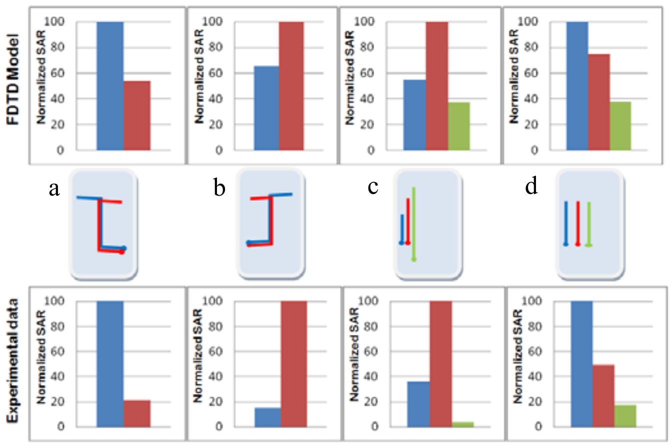

Fig. 8. Comparison between the SAR measured from the temperature increases recorded inside a laboratory RF coil and the SAR computed in the FDTD over equivalent implant configurations and RF exposure conditions. Note that each graph has been normalized to the related maximum value of SAR. The bar-plots refer to the implant configurations of the same color reported as x-axis.

C. *Heating in the HVD implanted with a PM*

The validated birdcage coil model was then integrated with the Human Visible dataset and a PM implant; in particular, a right and a left pectoral implant configuration were reproduced. Figure 9 reports SAR distribution over a frontal plane through the lead tip for the two cases.

The birdcage coil was excited by a quadrature voltage with an amplitude that induced a whole-body mean SAR of 1W kg^{-1} (value typically used in MRI thorax investigation) inside the HVD with no implant.

Under this excitation condition, a local SAR of 143.9 W kg^{-1}, averaged over 1mg of tissue, was computed for the right implant configuration. With the PM implanted in the left pectoral region, the computed SAR at the lead tip was significantly lower, i.e., 28.8 W kg^{-1}.

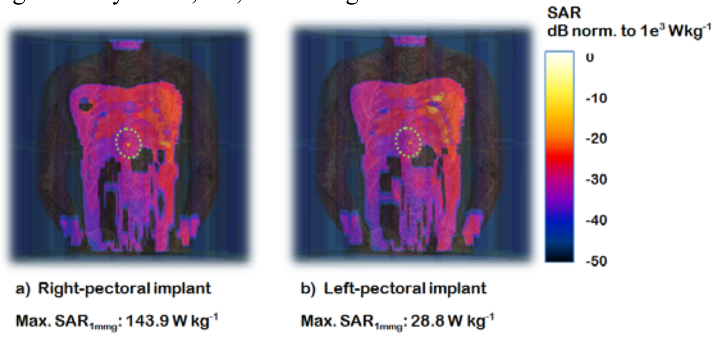

Fig. 9. Human Visible dataset implanted with a PM and exposed to the RF field of a birdcage coil: SAR distribution as resulting from the numerical model. a) right pectoral implant configuration; b) left-pectoral implant configuration. The dotted circles indicate the contact points between the lead tip and tissues.

IV. Discussion

Each year, approximately 1 million people worldwide are implanted with a PM, hundreds of thousands of whom might benefit from an MRI scan. A recent study [17] shows that an MRI procedure is requested by a physician for 17% of PM patients within 12 months of device implant. Every three minutes in the U.S. and every six minutes in Europe, a patient is denied an MRI scan due to the presence of a cardiac device.

Several studies have demonstrated the potential for MRI to be performed in PM or ICD patients without any serious clinical consequence [2,18,19]. As in previous studies, however, the authors acknowledge a multitude of limitations that prevent the broad applicability of the results, which makes further and more comprehensive investigations necessary.

With regards to MRI-induced heating on PM and ICD leads, the large number of variables that take part in the process makes it extremely difficult to perform extensive and exhaustive experimental measurements. Simulation approaches based on numerical tools may be a useful means to limit the number of experimental measurements and better identify the contribution of the various aspects involved. To get reliable results though, every numerical study needs an appropriate experimental validation.

The main finding of this study was that an accurate modeling of the actual physical and electrical structure of an MRI RF birdcage coil faithfully reproduced the thermal effects on metal implants.

A numerical model based on FDTD simulations was validated to obtain a general tool for investigating RF deposited power, and the role of the multiple parameters and factors involved in this complex phenomenon. For validation the numerical model of the MRI birdcage coil was compared it with an equivalent custom-designed physical structure. The most widely used whole-body birdcage coil in clinical MRI scanners are built using two tunable capacitors at the end of each leg and a distributed capacitance given by the geometry of the leg. The birdcage coil we built and modeled has three capacitors per leg, whereas the typical birdcage models proposed in the literature have a single capacitor per leg, regardless of the actual structure of the coil. Thus, our model most closely reproduces the structure of a real birdcage coil: the two capacitors between each leg and the ring model the tunable capacitors; the third capacitor in the middle of each leg models the distributed leg capacitance . Such a structure allows RF coil manufacturers to obtain a more uniform and symmetric field distribution.

Measurements of the reflection coefficient and the current along the legs of the coil showed that the FDTD model reproduced the behavior of the physical structure fairly well. The error between the numerical model and the experimental data was 3 dB (13%) for the reflection coefficient at 64MHz; the mean error for the current amplitude on the legs was 0.02 dB, ranging from -3.43 to 2.33 dB. No systematic under/overestimation was observed, but for the feeding legs whose currents were fairly overestimated by the numerical model.

Current phase distribution along the 16 legs was consistent with the circular-polarized magnetic field to be generated inside the coil: an almost constant 22.5° shift between two consecutive legs was measured in the numerical model of the head-sized coil. The physical model showed a similar behaviour: the mean error was 1.12% with respect to the turn angle, ranging from -3.96% to 6.01%. The highest error was observed at one of the legs where the RF signal was applied and at the ones opposing the RF ports.

The standard deviation of the experimental measurements is comparable with the accuracy of the current clamp probes (± 1dB). In most legs the differences between numerical and experimental data were within the measurement error, so that no systematic under/overestimation occurred. The highest differences were observed for the legs connected to the feeding points. In particular the numerical model shows a sharp increase in the current of the feeding legs respect to the adjacent ones, while a smoother distribution characterizes the physical model. We speculate that the numerical modeling might not take into account electrical losses, such as those of the feeding and matching circuits (e.g. phase shifter and baluns). This implies that, in the numerical model, the estimation of the EM field distribution in close proximity of the birdcage feeding legs may be inaccurate.

The whole-body birdcage coil model was obtained by scaling the head-sized coil, and the capacitor values were adapted to obtain the resonance at 64 MHz. The physical whole-body coil had the same structure as the head-sized coil, in terms of number of legs, number and position of the tuning capacitors, and feeding ports.

We compared the deposited power computed in the whole-body-sized coil model at the tip of the metal wires with a set of experimental data collected from the physical whole-body-sized coil. As experimental SAR values were calculated from the slope of the initial temperature rise, they contain an error associated with the size of the temperature probe and with the methods for SAR evaluation itself [4,6]. In addition, in the numerical model it is difficult to define an optimal averaging mass for SAR evaluation, that may be suitably compared with the experimental data. Despite these limitations, the proposed numerical model consistently reproduced the effects of those factors that in the experimental study [6] played a major role in heat induction (e.g. implant location, geometry and length).

SAR distribution as computed inside the Human Visible implanted with the PM and its lead showed that implant positioning is an important aspect that can have an effect the amount of heat induced at the lead tip. Today, the site for PM location (left or right pectoral region) is the surgeon's choice, without any relevant clinical motivation. Our data show that the PM implanted in the left-pectoral region causes a SAR deposition level at the lead tip of about 20% the local maximum SAR peak at the right-pectoral implant. This suggests that the left pectoral region is somehow to be preferred as location for a PM implant. The asymmetric distribution of the electric field within the body [20], and the better coupling of the right-implant lead with the currents induced in the biological tissues [6] can justify such behavior. Experimental data collected on homogeneous phantoms implanted with PMs in different configurations [3,5,6,20] confirm these data. The numerical approach adopted in this study accounts for several aspects that experiments on homogenous gel phantoms may not: in particular, designing a path for the PM lead that follows the anatomical structure of blood vessels, and modeling different tissues with different electromagnetic properties, make the analysis more realistic, extend the range of experimental measurements, and help correlate heating results to those expected in humans.

A limitation of our study is that we did not model the heat transfer mechanisms that living tissues enact in order to keep their temperature within a given range. Such a limitation precludes the immediate association of the computed SAR with the actual temperature increase and tissue damage. In any case, the validation made in terms of electrical parameters and SAR makes our model suitable for future studies on heat transfer mechanisms and tissue damage. Still, the model we developed is a useful tool to evaluate potential safety issues regarding MRI-induced heating in implanted patients. In particular, it allows the physician to balance advantages and disadvantages associated with a particular implant configuration in terms of implant location, implant geometry and total-body deposited power, and eventually plan an MRI scan also in the presence of an implanted cardiac device without posing a real risk for the patient.

V. Conclusions

The SAR distribution computed for the two typical implant configurations (left and right pectoral regions) reveal that implant location is an important aspect that affects the amount of induced heating at the lead tip. In particular, temperature increase seems to be lower in a left pectoral implant than in a right one.

The numerical model we developed is a useful tool to study the peculiarity of specific implant configurations and predict the induced SAR in the surrounding tissues. The validation of the model by experimental measurements confirmed the reliability of the numerical results.

This accurate numerical model could also be used as a reference for validating simpler models to reduce the computational effort. Such simplifications might involve the reduction of the number of lumped elements, the type of RF sources, and a coarser simulation of the structure of the coil.

The FDTD model is freely available to other researchers or to the industry upon request.

ACKNOWLEDGMENT

The Authors wish to thanks Howard Bassen and Wolfgang Kainz of the Center for Devices and Radiological Health of the Food and Drug Administration for their help in collecting the data on the whole-body coil; Monica Brocco and Giorgio De Angelis of the Dept. of Technology and Health of the Italian National Institute of Health for the linguistic revision of the manuscript and for the construction of the head-sized birdcage coil prototype, respectively.

REFERENCES

[1] T Sommer , C Vahlhaus, G Lauck, A von Smekal, M Reinke, U Hofer, W Block, F Traber, C Schneider, J Gieseke, W Jung, H Schild: MR imaging and cardiac pacemakers: in-vitro evaluation and in-vivo studies in 51 patients at 0.5 T. *Radiology* 2000, **215**(3):869-79

[2] A Roguin, MM Zviman, GR Meininger, ER Rodrigues, TM Dickfeld, DA Bluemke, A Lardo, RD Berger, H Calkins, HR Halperin: Modern pacemaker and implantable cardioverter/defibrillator systems can be magnetic resonance imaging safe: in vitro and in vivo assessment of safety and function at 1.5 T. *Circulation* 2004, **110**(5):475-82. 2004 Aug 3

[3] H Bassen, W Kainz, G Mendoza, T Kellom: MRI-induced heating of selected thin wire metallic implants – laboratory and computational studies – findings and new questions raised. *Minim Invasive Ther Allied Technol* 2006, **15**(2):76-84

[4] E Mattei, M Triventi, G Calcagnini, F Censi, W Kainz, HI Bassen, P Bartolini: Temperature and SAR measurement errors in the evaluation of metallic linear structures heating during MRI using fluoroptic probes. *Phys Med Biol* **52**(6):1633-46. 2007 Mar 21

[5] G Calcagnini, M Triventi, F Censi, E Mattei, P Bartolini, W Kainz, HI Bassen. In vitro investigation of pacemaker lead heating induced by magnetic resonance imaging: role of implant geometry. *J Magn Reson Imaging*. 2008 Oct;**28**(4):879-86

[6] E Mattei, M Triventi, G Calcagnini, F Censi, W Kainz, G Mendoza, HI Bassen, P Bartolini. Complexity of MRI induced heating on metallic leads: experimental measurements of 374 configurations *Biomed Eng Online*. 2008 Mar 3;**7**:11

[7] TS Ibrahim, C Mitchell, P Schmalbrock, R Lee, DW Chakeres. Electromagnetic perspective on the operation of RF coils at 1.5-11.7 Tesla. *Magn Reson Med*. 2005 Sep;**54**(3):683-90

[8] TS Ibrahim, R Lee, BA Baertlein, Y Yu, PM Robitaille. Computational analysis of the high pass birdcage resonator: finite difference time domain simulations for high-field MRI. *Magn Reson Imaging* 2000; **18**:835–843

[9] KS Yee. Numerical solution of initial boundary value problems involving Maxwell's equations in isotropic media. *IEEE Trans Antenna Propag* 1966;**4**:302–307

[10] JM Jin, J Chen, WC Chew, H Gan, RL Magin, PJ Dimbylow. Computation of electromagnetic fields for high-frequency magnetic resonance imaging applications. *Phys Med Biol* 1996;41:2719–2738.

[11] CM Collins, SL Li, MB Smith. SAR and B1 field distributions in a heterogeneous human head model within a birdcage coil. *Magn Reson Med* 1998;**40**:846–856

[12] EC Hayes, WA Edelstein, DF Schenck, OM Mueller, M Eash. An efficient highly homogeneous radiofrequency coil for whole-body NMR imaging at 1.5 T. *J Magn Reson* 1985;**63**:622–628

[13] JT Vaughan, HP Hetherington, JO Otu, JW Pan, JM Pohost. High frequency volume coils for clinical NMR imaging and spectroscopy. *Magn Reson Med* 1994;**32**:206–218

[14] TS Ibrahim, R Lee, BA Baertlein, AM Abduljalil, H Zhu, PM Robitaille. Effect of RF coil excitation on field inhomogeneity at ultra high fields: a field optimized TEM resonator. *Magn Reson Imaging* 2001;**19**:1339–1347

[15] TS Ibrahim, R Lee, BA Baertlein, PM Robitaille. Application of finite difference time domain method for the design of birdcage RF head coils using multi-port excitations. *Magn Reson Imaging* 2000;**18**:733–742

[16] IEEE, IEEE1528, recommended practice for determining the spatial-peak specific absorption rate (SAR) in the human body due to wireless communications devices: Measurement techniques, IEEE Standards Department 52(5), 12006

[17] E Mattei, M Triventi, G Calcagnini, F Censi, P Bartolini. Radiofrequency Dosimetry in Subjects Implanted with Metallic Structures Undergoing MRI: a Numerical Study Am. J. Biomed. Sci. 2009, 1(4), 373 – 384

[18] C95.3-2003: Recommended Practice for Measurements and Computations with Respect to Human Exposure to RadioFrequency Electromagnetic Fields, 100 kHz to 300 GHz, Institute of Electrical and Electronics Engineers (EEEI)

[19] ASTM F2182–02a – ''Standard Test Method for Measurement of Radio Frequency Induced Heating Near Passive Implants During Magnetic Resonance Imaging'', *ASTM International*, 100 Barr Harbor Drive, PO Box C700, West Conshohocken, PA, 19428–2959 USA

[20] T Sommer, CP Naehle, A Yang, V Zeijlemaker, M Hackenbroch, A Schmiedel, C Meyer, K Strach, D Skowasch, C Vahlhaus, H Litt, H Schild. Strategy for safe performance of extrathoracic magnetic resonance imaging at 1.5 tesla in the presence of cardiac pacemakers in non-pacemaker-dependent patients: a prospective study with 115 examinations. *Circulation*. 2006 Sep 19;**114**(12):1285-92

[21] ET Martin, JA Coman, FG Shellock, CC Pulling, R Fair, K Jenkins. Magnetic resonance imaging and cardiac pacemaker safety at 1.5-Tesla. *J Am Coll Cardiol*. 2004;**43**:1315–1324

[22] JR Gimbel, E Kanal, KM Schwartz, BL Wilkoff. Outcome of magnetic resonance imaging (MRI) in selected patients with implantable cardioverter defibrillators (ICDs). *Pacing Clin Electrophysiol*. 2005;**28**:268–269

[23] P Nordbeck, F Fidler, I Weiss, M Warmuth, MT Friedrich, P Ehses, W Geistert, O Ritter, PM Jakob, ME Ladd, HH Quick, WR Bauer. Spatial distribution of RF-induced E-fields and implant heating in MRI. *Magn Reson Med*. 2008 Aug;**60**(2):312-9